Photoacoustics 26 (2022) 100364

Contents lists available at ScienceDirect

Photoacoustics

journal homepage: www.elsevier.com/locate/pacs

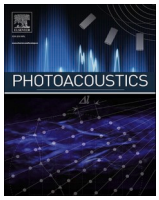

Spectroscopic photoacoustic microscopic imaging during single spatial scan using broadband excitation light pulses with wavelength-dependent time delay

Takeshi Hirasawa [a], Kazuyoshi Tachi [a,b], Manami Miyashita [a], Shinpei Okawa [a], Toshihiro Kushibiki [a], Miya Ishihara [a,*]

[a] Department of Medical Engineering, National Defense Medical College, 3–2 Namiki, Tokorozawa, Saitama 359–8513, Japan
[b] Department of Urology, National Defense Medical College, 3–2 Namiki, Tokorozawa, Saitama 359–8513, Japan

ARTICLE INFO

Keywords:
Photoacoustic microscopy
Photoacoustic imaging
Spectroscopic imaging
Multispectral imaging
Supercontinuum light

ABSTRACT

In most multispectral optical-resolution photoacoustic microscopy (OR-PAM), spatial scanning is repeated for each excitation wavelength, which decreases throughput and causes motion artifacts during spectral processing. This study proposes a new spectroscopic OR-PAM technique to acquire information on the photoacoustic signal intensity and excitation wavelength from single spatial scans. The technique involves irradiating an imaging target with two broadband optical pulses with and without wavelength-dependent time delays. The excitation wavelength of the sample is then calculated by measuring the time delay between the photoacoustic signals generated by the two optical pulses. This technique is validated by measuring the excitation wavelengths of dyes in tubes. Furthermore, we demonstrate the three-dimensional spectroscopic OR-PAM of cells stained with suitable dyes. Although the tradeoff between excitation efficiency and excitation bandwidth must be adjusted based on the application, combining the proposed technique with fast spatial scanning methods can significantly contribute to recent OR-PAM applications, such as monitoring quick biological events and microscale tracking of moving materials.

1. Introduction

Optical-resolution photoacoustic (PA) microscopy (OR-PAM) is a technique for imaging optical absorbers inside biological tissues using microscopic spatial resolution [1,2]. In OR-PAM, pulsed excitation light is irradiated on the sample. An acoustic sensor detects the PA signals produced from the optical absorbers. The PA signal intensity is proportional to the optical energy absorbed by the optical absorbers, reflecting their optical absorption coefficients. Therefore, optical absorbers, including hemoglobin, melanin, lipids, and exogenous contrast agents, can be distinguished by measuring the PA signals at multiple excitation wavelengths, also called multispectral PAM. Multispectral PAM has been applied in blood vessel imaging [1,3], oxygen metabolism measurements [4–7], melanoma diagnosis [4,8,9], and contrast agent imaging [10]. In recent years, researchers have studied high-throughput imaging techniques for wide-field imaging of transient events in biological tissues, including drug responses [11] and brain functions [12]. In multispectral PAM, the throughput is determined by spatial and wavelength scanning. For spatial scan, fast scanning techniques that use water-immersible MEMS mirrors [13,14] or water-immersible polygonal mirrors [11,15] have been developed. However, for wavelength scanning, most studies involve serial scanning, which requires multiple spatial scans to collect the PAM images at multiple excitation wavelengths. Thus, the throughput decreases, resulting in motion artifacts because of the translation of the optical absorbers during spatial scanning at each excitation wavelength. To perform fast wavelength scanning, techniques have been proposed using multiple lasers synchronized to irradiate light pulses alternately during spatial scanning [12]. Another technique uses an electro-optic modulator to quickly control the optical path before the wavelength conversion part of the lasers

Abbreviations: **PA**, Photoacoustic; **PAM**, Photoacoustic microscopy; **OR-PAM**, Optical-resolution PAM; **MEMS**, Micro-electro-mechanical systems; **SC**, Supercontinuum; **SMF**, Single-mode fiber; **DMSO**, Dimethyl sulfoxide; **ND**, Neutral-density; **HBSS**, Hanks' balanced salt solution.

* Corresponding author.
E-mail addresses: hirasawa@ndmc.ac.jp (T. Hirasawa), doc31234@ndmc.ac.jp (K. Tachi), miyashitam@ndmc.ac.jp (M. Miyashita), okawa@hama-med.ac.jp (S. Okawa), toshi@ndmc.ac.jp (T. Kushibiki), miyaishi@ndmc.ac.jp (M. Ishihara).

https://doi.org/10.1016/j.pacs.2022.100364
Received 31 January 2022; Received in revised form 15 April 2022; Accepted 29 April 2022
Available online 4 May 2022

[16–18]. The technique using a Raman scattering fiber laser with optical delay lines that emit multiple-wavelength excitation lights with time delays [10,11,19,20] has also been proposed. However, the number and range of excitation wavelengths are determined by the laser wavelengths, thus limiting the corresponding numbers and excitation wavelengths of the optical absorbers. As a result, despite the advantages of relatively low light scattering and low intrinsic signals from hemoglobin, multispectral PAM systems that can image contrast agents that absorb near-infrared light (except for 1064 nm) are limited [21]. To overcome this problem, this study presents a spectroscopic OR-PAM technique that operates over a wide range of optical wavelengths and offers continuous spectral information during single spatial scanning.

The proposed spectroscopic OR-PAM uses nanosecond pulsed supercontinuum (SC) light as the excitation source. Recently, some studies have successfully used the nanosecond SC light source for multispectral PAM [22–30]. The studies have used narrowband light extracted from the SC light for excitation, and its wavelength range was easily selected using bandpass filters. In the proposed spectroscopic OR-PAM, the broadband excitation light pulse produced by a nanosecond pulsed SC light source is split into two optical paths. One is passed through a long single-mode fiber (SMF), introducing the wavelength-dependent time delay before the light pulses are combined. The interval between the two combined pulses depends on the wavelength, thus enabling the convolution of optical absorption's spectroscopic information into PA signals. Therefore, we have obtained data on optical absorption at continuous excitation wavelengths by measuring a couple of PA signals produced by the broadband excitation light pulse with and without wavelength-dependent time delay. This study reports the development of the proposed spectroscopic OR-PAM system and its experimental validation using tube phantoms and three-dimensional cultured cells.

2. Theory

2.1. Spectroscopic OR-PAM

In the proposed OR-PAM, the PA signal produced by the optical absorbers irradiated by excitation light is detected using an acoustic sensor. The pressure of the PA signal is expressed as

$$c^2\nabla^2 p(\mathbf{r},t) - \frac{\partial^2}{\partial t^2}p(\mathbf{r},t) = \Gamma\cdot\eta\cdot\frac{\partial}{\partial t}a(\mathbf{r},t), \tag{1}$$

where η is the conversion efficiency from optical energy to heat, Γ is the Grüneisen parameter representing the conversion efficiency from heat to pressure, c is sound speed, and $a(\mathbf{r},t)$ is the optical energy absorbed by the optical absorbers [31–33]. Under the condition that the pulse width of the laser is much shorter than the thermal diffusion time of the optical absorbers, the PA signal at the origin of the coordinate can be written as

$$p(t) = \frac{\Gamma\cdot\eta}{4\pi c^2}\iiint\frac{d\mathbf{r}}{r}\frac{\partial}{\partial t'}a(\mathbf{r},t')\Big|_{t'=t-\frac{r}{c}}, \tag{2}$$

where $r = |\mathbf{r}|$ [34,35]. The optical energy absorbed by the optical absorbers $a(\mathbf{r},t)$ can be expressed as $a(\mathbf{r},t) = a(\mathbf{r})\ i(t)$, where $a(\mathbf{r})$ is the spatial distribution of the absorbed optical energy and $i'(t)$ is the first derivative of the excitation light pulse. Eq. (2) can be rewritten in spherical coordinates as proposed in the papers [31–33].

$$\begin{aligned} p(t) &= \frac{\Gamma\cdot\eta}{4\pi c^2}\int\left(\frac{1}{r}\iint a(r,\theta,\phi)r^2\sin\theta d\theta d\phi\right)i'\left(t-\frac{r}{c}\right)dr \\ &= \frac{\Gamma\cdot\eta}{4\pi c^2}\int\left(\frac{1}{t'}\iint a(ct',\theta,\phi)(ct')^2\sin\theta d\theta d\phi\right)i'(t-t')dt' \\ &= \frac{\Gamma\cdot\eta}{4\pi c^2}\left(\frac{1}{t}\iint_{r=ct}a(\mathbf{r})dS\right)*i'(t) \end{aligned} \tag{3}$$

The PA signal at the origin of the coordinate $p_{bb}(t)$ is expressed as [28] for excitation light with a broadband spectral bandwidth.

$$p_{bb}(t) = \frac{\Gamma\cdot\eta}{4\pi c^2}\left(\frac{1}{t}\iint_{r=ct}\int a(\mathbf{r},\lambda)\,d\lambda\,dS\right)*i'(t), \tag{4}$$

where λ is the optical wavelength. For broadband spectral bandwidth excitation light with wavelength-dependent time delay, the source pressure $p_{td}(\mathbf{r},\lambda,t)$ is expressed as

$$p_{td}(t) = \frac{\Gamma\cdot\eta}{4\pi c^2}\int\left(\frac{1}{t}\iint_{r=ct}a(\mathbf{r},\lambda)dS\right)*i'(t-\alpha\lambda)\,d\lambda, \tag{5}$$

where α is the chromatic dispersion per optical wavelength. Assuming that the wavelength dependence of the absorbed optical energy is constant within a small volume, the optical energy absorbed by the optical absorbers $a(\mathbf{r},\lambda)$ can be expressed as $a(\mathbf{r},\lambda) = a(\mathbf{r})\ b(\lambda)$, where $a(\mathbf{r})$ is the spatial distribution of the absorbed optical energy and $b(\lambda)$ is the wavelength dependence of the absorbed optical energy, which is normalized as $\int b(\lambda)d\lambda = 1$. With this assumption, Eq. (6) can be rewritten as

$$\begin{aligned} p_{td}(t) &= \frac{\Gamma\cdot\eta}{4\pi c^2}\int\left(\frac{1}{t}\iint_{r=ct}a(\mathbf{r})b(\lambda)dS\right)*i'(t-\alpha\lambda)\,d\lambda \\ &= \frac{\Gamma\cdot\eta}{4\pi c^2}\int\left(\frac{1}{t}\iint_{r=ct}a(\mathbf{r})dS\right)*\int b(\lambda)\cdot i'(t-\alpha\lambda)d\lambda \\ &= \alpha\cdot b(\alpha\lambda)*p_{bb}(t) \end{aligned} \tag{6}$$

where α is the chromatic dispersion per optical wavelength. This equation indicates that the wavelength dependence of the absorbed optical energy $b(\lambda)$ is convolved with the pressure source. The frequency spectra of the PA signals $S_{bb}(f)$ and $S_{td}(f)$ detected by the acoustic sensor at the origin can be calculated from the product of the Fourier transforms of the initial pressures $P_{bb}(f)$ and $P_{td}(f)$ by the wavelength-independent system function $G(f)$, representing the acoustic attenuation during propagation from the source to detector, detector frequency sensitivity characteristic, and detector directionality [36,37]. Although various factors affect the PA signal, the effects of factors that are independent of the optical wavelength are canceled by calculating the ratio of the frequency spectra, and the equation becomes

$$\frac{S_{td}(f)}{S_{bb}(f)} = \frac{P_{td}(f)\cdot G(f)}{P_{bb}(f)\cdot G(f)} = \alpha\cdot F[b(\alpha\lambda)]. \tag{7}$$

Therefore, the wavelength dependence of the absorbed optical energy can be theoretically obtained by deconvolving the PA signals produced by the broadband excitation light without the wavelength-dependent time delay from those produced by the broadband excitation light with the wavelength-dependent time delay. For imaging targets with multiple optical absorbers having different absorption spectra, the frequency spectra of the signals from each optical absorber should be calculated separately using short-time Fourier transforms. Deconvolution processing requires signals with high signal-to-noise characteristics. Therefore, cross-correlation was used to measure the time delay between two signals and calculate the excitation wavelengths that contribute to PA signal generation.

2.2. Two-dimensional colormap for visualization of spectroscopic OR-PAM

To visualize the dual information of the excitation wavelength and signal intensity as a single image, we employ a two-dimensional colormap using the hue, saturation, and lightness (HSL) color space, with $H \le H_{max}$, $S = 1$, and $L \le 0.5$ and calculated as [38].

$$H = H_{\max} - (\lambda_{ex} - \lambda_{\min})/(\lambda_{\max} - \lambda_{\min})\cdot H_{\max}, \tag{7}$$

$$C = 2\cdot L = (S - S_{\min})/(S_{\max} - S_{\min}), \tag{8}$$

$$X = C\cdot[1 - |\{(H/60)\bmod 2\} - 1|\,], \tag{9}$$

$$(R,G,B) = \begin{cases} (\ C,\ X,\ 0\ ) & 0 \le H < 60 \\ (\ X,\ C,\ 0\ ) & 60 \le H < 120 \\ (\ 0,\ C,\ X\ ) & 120 \le H < 180 \\ (\ 0,\ X,\ C\ ) & 180 \le H < 240 \\ (\ X,\ 0,\ C\ ) & 240 \le H < 300 \\ (\ C,\ 0,\ X\ ) & 300 \le H < 360 \end{cases}, \tag{10}$$

where S and λ_{ex} are the intensity and excitation wavelength of the PA signal. S_{min} and S_{max} are the minimum and maximum intensity color scales of the PA signal, respectively. λ_{max} and λ_{min} are the minimum and maximum of the excitation wavelength color scale, respectively. The maximum hue value H_{max} controls the colormap hue range, i.e., from red to violet when $H_{max} = 300$ and from red to blue when $H_{max} = 240$.

3. Materials and methods

3.1. Experimental setup for spectroscopic OR-PAM

Fig. 1 shows the experimental setup for spectroscopic OR-PAM. An SC light source (SC-Pro-HP, YSL photonics, Wuhan, China) produced broadband excitation light. The SC light was collimated using a built-in collimator, filtered using a cold filter (SC1101, Asahi Spectra, Tokyo, Japan), and a bandpass filter consisting of a pair of a long pass filter (FELH0600, Thorlabs, Newton, NJ), and a short pass filter (FESH900, Thorlabs, Newton, NJ). The SC light was guided into a 70/30 single-mode coupler (45-U7975–30–22031, Gould Fiber Optics, Millersville, MD) using an achromatic focusing lens (AC060–010-B-ML, Thorlabs, Newton, NJ). The 30% output of the single-mode coupler was connected to the 30% input of another single-mode coupler. The 70% output of the single-mode coupler was in turn connected to a long SMF (630HP, 1 km, Thorlabs, Newton, NJ) to produce the wavelength-dependent time delay; the output of the long optical fiber was connected to the 70% input of the single-mode coupler. Broadband excitation light pulses with and without wavelength-dependent time delays were emitted from the output of the single-mode coupler. The light pulses were used as excitation light for an OR-PAM system based on a Core Unit Microscope (CUS-BF, SigmaKoki, Tokyo, Japan). The output of the single-mode coupler was connected to a reflective fiber collimator (RC04FC-P01, Thorlabs, Newton, NJ). The excitation light emitted from the collimator was passed through a filter wheel (FW2A, Thorlabs, Newton, NJ) mounted with 50 nm bandwidth bandpass filters having central wavelengths of 650, 700, 750, 800, and 850 nm (#84–786, #84–787, #84–788, #84–789, #84–790, Edmund Optics, Barrington, NJ). For the spectroscopic OR-PAM using a broadband light pulse, the excitation light was passed through an empty port of the filter wheel. The excitation light was passed through a port with one of the bandpass filters for the multispectral PAM using narrowband light pulses or excitation light validation. For adjusting the excitation light power, the excitation light was passed through a tunable neutral-density filter (NDHN-U100, SigmaKoki, Tokyo, Japan) and reflected by a dichroic shortpass mirror with a cut-off wavelength of 550 nm (#69–215, Edmond Optics, Barrington, NJ). The light was then focused on the sample using an objective lens with a focal length of 40 mm and a numerical aperture of 0.13 (EPL-5, SigmaKoki, Tokyo, Japan). The sample was then immersed in water, and the PA signal produced from the sample was measured using a focused acoustic sensor made of P(VDF-TrFE) film (KF-2#10-PI5-φ3-SR5-SMA, ELMECH Co., Ltd., Niigata, Japan). The acoustic sensor parameters included the focal length, element diameter, and central frequency of 5.0 mm, 3.0 mm, and 40 MHz. The PA signal measured by the acoustic sensor was amplified using two amplifiers (SA-230F5, NF Corporation, Kanagawa, Japan), filtered using a highpass filter with a cut-off frequency of 1.8 MHz (EF509, Thorlabs, Newton, NJ), and recorded by a digital oscilloscope (PXIe-5164, National Instruments, Austin, TX) operating at a sampling frequency of 500 MHz. The sample was raster-scanned using a pair of motorized stages (OSMS26–50 and HPS80–50X-M5, SigmaKoki, Tokyo, Japan). The position of the motorized stage was monitored by a linear gauge (LGK-0110, Mitutoyo Corporation, Kanagawa, Japan) and an analog counter (ELVIS II+, National Instruments, Austin, TX) to compensate for the image distortions caused by slight fluctuations in the stage translation speed and translation time delay (time delay between software trigger and stage translation). The motorized stage, digital oscilloscope, light source, and analog counter were synchronized with a LabVIEW program. The PA signals were enveloped using the Hilbert transform to calculate the intensities [39]. Image distortion because of fluctuation in the stage translation speed was compensated using a linear gauge. To improve the signal-to-noise ratio, two-dimensional Gaussian filtering was applied on the XY plane.

3.2. Evaluation of the time-delayed excitation light

The excitation light pulses emitted from the output of the single-mode coupler were filtered using the bandpass filter and measured by a biplanar phototube (R1328U-51, Hamamatsu Photonics KK, Shizuoka, Japan) at the output of the objective lens. Then, the light pulses were recorded by the digital oscilloscope (PXIe-5164, National Instruments, Austin, TX) operating at a sampling frequency of 1 GHz with a signal averaging 64 times. The light pulse comprised primary and secondary light pulses without and with wavelength-dependent time delays. The wavelength-dependent time delay between the two pulses τ was the propagation time of the light through the long SMF, expressed as $\tau = L/$

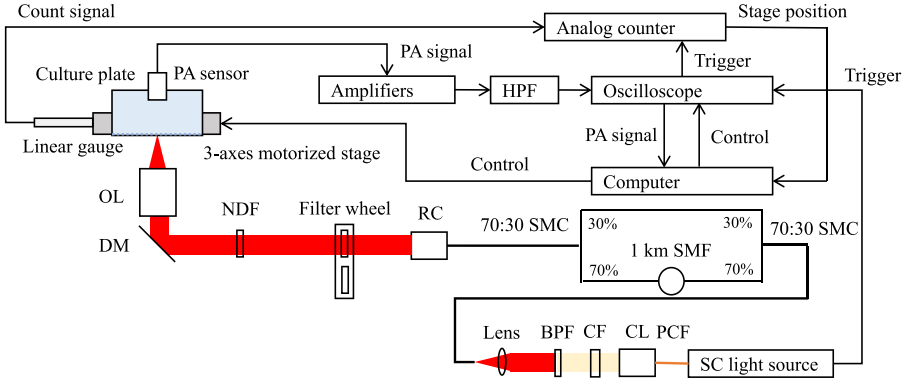

Fig. 1. Schematic of the experimental setup for spectroscopic OR-PAM SC: Supercontinuum; PCF: Photonic crystal fiber; CL: Collimator lens; CF: Cold filter; BPF: Bandpass filter; SMF: Single-mode fiber; SMC: Single-mode coupler; RC: Reflective collimator; NDF: Neutral-density filter; OL: Objective lens; DM: Dichroic mirror; HPF: Highpass filter.

(c_0/n_f), where L is the SMF length, c_0 is the speed of light in a vacuum, and n_f is the refractive index of the SMF core. Considering that the refractive index of the SMF depends on the wavelength, the time delay τ is wavelength-dependent. We calculated the time delay based on the specifications of the SMF obtained from the manufacturer and compared these values with the measured values. The excitation light energy was measured using a laser power meter (Nova II, Ophir Optronics, Jerusalem, Israel) with a photodiode sensor (PD300, Ophir Optronics, Jerusalem, Israel).

3.3. Evaluation of spatial resolution

The proposed OR-PAM imaged a chrome-coated USAF 1951 test target (#58–198, Edmund Optics, Barrington, NJ) to evaluate the spatial resolution. The imaging area included elements 5 and 6 of group 3 in the test target. The line pitches of those elements were 12.7 mm^{-1} and 14.3 mm^{-1}. The test target was pasted to the bottom of a 100 mm cell-culture dish (3020–100, AGC Techno Glass Co. Ltd., Shizuoka, Japan). The dish was placed on the sample holder mounted on the motorized stage of the OR-PAM and filled with distilled water. The excitation light filtered by a 50 nm bandwidth bandpass filter (#84–788, Edmund Optics, Barrington, NJ) with a central wavelength of 750 nm was focused on the bottom of the dish; the acoustic sensor detected the PA signal produced from the sample. The excitation light's average power and repetition frequencies were 0.3 mW and 100 kHz. The dish was raster-scanned over an area of 640 × 640 μm in 2 μm steps to acquire the three-dimensional image of the tubes. The PA signals were averaged 64 times to reduce random noise. The full width at half maximum was calculated to measure the spatial resolution by fitting the signal intensities along the x-axis to an edge-spread function.

3.4. Spectroscopic OR-PAM of a phantom

Dye solutions with known absorption spectra—IRDye800CW solution (1 mM in DMSO, IRDye800CW Carboxylate, LI-COR, Inc., Lincoln, NE) and StellaFluor700 solution (1 mM in DMSO, StellaFluor700-COOH, Goryo Chemical, Hokkaido, Japan)—were measured by the proposed spectroscopic OR-PAM to test whether the spectroscopic OR-PAM could obtain the spectral information of samples. The dye solutions were stored in thin polytetrafluoroethylene tubes with inner and outer diameters of 51 μm and 153 μm, respectively (SLW-AWG44, Hagitec Co. Ltd., Chiba, Japan). The tubes were pasted at the bottom of a 100 mm cell culture dish (3020–100, AGC Techno Glass Co. Ltd., Shizuoka, Japan). The dish was placed on the sample holder mounted on the motorized stage of the OR-PAM and filled with distilled water. The excitation light was focused on the bottom of the dish; the acoustic sensor detected the PA signal produced from the sample. The dish was raster-scanned within the area of 640 × 80 μm^2 in 2 μm steps to acquire the three-dimensional image of the tubes. The PA signals were averaged 256 times to reduce random noise. Furthermore, the excitation light was attenuated by the tunable ND filter to 20% of the power measured to prevent saturation of the amplifier. This process is explained in detail in Section 3.2.

The PA signal produced by the primary light pulse was cropped in the range of ± 30 ns from its maxima to calculate the excitation wavelengths. We calculated the cross-correlation of the cropped PA signal and the PA signal produced by the secondary light pulse to determine the time delay that maximizes the cross-correlation. The excitation wavelength was calculated using the time delay, and the excitation wavelength was measured using the method described in Section 3.2. Since signal enveloping decreases the time resolution of the cross-correlation, the excitation wavelength of the PA signal was calculated before enveloping.

Finally, we measured the absorption spectra of the solutions diluted to 10 μM in DMSO using a spectrophotometer (UV1900, Shimadzu Corp., Kyoto, Japan) with a super micro black cell (200–55678–11, Shimadzu Corp., Kyoto, Japan) to compare the excitation wavelengths measured from the spectroscopic OR-PAM and absorption spectra of the solutions.

3.5. Spectroscopic OR-PAM of cultured cells

Human cervical cancer cells (HeLa cells) stained using cell-staining dyes of various excitation wavelengths were imaged to demonstrate that the proposed spectroscopic OR-PAM technique can differentiate cells based on their excitation wavelengths. The HeLa cells were grown in Dulbecco's modified Eagle's medium (DMEM) containing D-glucose, L-glutamine, and sodium pyruvate (11885–084; Life Technologies, Carlsbad, CA, USA) and supplemented with 10% fetal bovine serum (FBS, SH3091003; Life Technologies, Carlsbad, CA, USA) and 1% antibiotic-antimycotic (15240–062; Life Technologies, Carlsbad, CA, USA) in 5% CO_2. The cells were divided into four centrifuge tubes and pelleted by centrifugation at 300 G for 4 min. The supernatants were removed from the tubes, and the cells were then resuspended in Hanks' balanced salt solution (HBSS) containing 0.25% of a cell-staining dye (Cell Brite Red, Biotium, Fremont, CA) or 5 μM of cell-staining dyes (CellBrite NIR680, CellBrite NIR750, CellBrite NIR790, Biotium, Fremont, CA). The excitation wavelengths of CellBrite Red, CellBrite NIR680, CellBrite NIR750, and CellBrite NIR790 are 644 nm, 683 nm, 748 nm, and 786 nm, respectively. The suspended cells were incubated for 4 h, washed two times by repeating centrifugation at 300 G for 2 min, and resuspended. Finally, the cells stained by various cell-staining dyes were mixed. The cells were seeded in a 12-well plate, incubated overnight, and used for the experiment for planar cultured cells. For the Matrigel suspension, the cells were mixed with Matrigel at a cell concentration of 4×10^6 cells/mL, dropped on the 12-well plate, and hardened by incubation for 30 min

The 12-well plate was placed on the sample holder of the OR-PAM instrument to obtain the spectroscopic OR-PAM images of the cells. The well plate was filled with HBSS, and the acoustic sensor was immersed in the HBSS. The excitation light was irradiated on the cells from the bottom of the plate. The focal plane of the excitation light was the bottom of the plate and the plane 200 μm above the bottom of the plate for the planar cultured cells and Matrigel suspension, respectively. The step size of the raster scanning was 2 μm. The PA signals were averaged 64 times to reduce random noise. Considering that cell-staining dyes do not absorb light with wavelengths over 850 nm, the longer limit of the excitation wavelength range was changed from 900 nm to 850 nm by replacing the short pass filter with another filter (FESH850, Thorlabs, Newton, NJ) with a cut-off wavelength of 850 nm. The C-scan spectroscopic OR-PAM images of the Matrigel suspensions were acquired by repeating the process described in Section 3.3 on the partial three-dimensional images cropped from the three-dimensional OR-PAM image in the z-axis range of ± 60 μm. The center depths of the partial three-dimensional images were incremented with a 60 μm step, and hence, each image had 60 μm overlaps. Before performing the spectroscopic OR-PAM imaging, the cells were imaged by fluorescence

Table 1
Fluorescence microscope filters used for four-color imaging.

Cell-staining dye	Excitation filter	Dichroic mirror	Emission filter	Filter set
CellBrite Red	620 (60)	660	700 (75)	Cy5, Nikon, Tokyo, Japan
CellBrite NIR690	655 (40)	685	716 (40)	Cy5.5-C, Semrock, Lake Forest, IL
CellBrite NIR750	716 (40)	757	775 (46)	#67–039, #87–066, #84–106, Edmund Optics, Barrington, NJ
CellBrite NIR790	769 (41)	801	832 (37)	#86–381, Edmund Optics, Barrington, NJ

microscopy. Table 1 summarizes the characteristics of the four-color fluorescence images acquired using the filters.

4. Results

4.1. Evaluation of the time-delayed excitation light

Fig. 2(a) shows the temporal waveforms of the excitation light pulses measured at the output of the objective lens. The excitation light pulses were filtered using BPFs with various transmission wavelengths to demonstrate the wavelength-dependent time delay; primary and secondary light pulses were observed in the waveform. The measured time delay was almost the same as the calculated value of 4.88 μs, within an error of 1.0%. No apparent time delays were observed in the wavelength ranges in the primary light pulse's magnified waveform (Fig. 2(b). Conversely, as shown in Fig. 2(c), the secondary pulse's wavelength-dependent time delay indicated that the long SMF had produced the wavelength-dependent time delay. As shown in Fig. 2(d), the wavelength dependence of the time delay between the two pulses was linearly correlated with the values calculated from the dispersion characteristic of the SFM ($R^2 = 0999$). The wavelength dependence of the time delay between the two pulses, as shown in Fig. 2(e), enables the calculation of the excitation wavelength of the optical absorber from the time delay between the PA signals produced by the two light pulses. The second-order polynomial fitting coefficients C_0, C_1, and C_2 were calculated as 1.874×10^6, -7.555×10^5, and 7.615×10^4, respectively.Fig. 2.

4.2. Evaluation of spatial resolution

Fig. 3(a) shows the maximum amplitude projection OR-PAM image of the test target. Fig. 3(b) shows the result of fitting the profile at the edge of the chrome pattern to the edge-spread function. The lateral resolution of 11.47 ± 0.98 μm was determined from the results of the fitting processing performed on 86 lines. The lateral a was almost precise as the diffraction-limited spot size of the optical focus (11.34 μm) was calculated as 0.51λ/NA [2,40], where NA was the numerical aperture. The numerical aperture of 0.034 was calculated from the beam diameter on the objective lens's input (2.7 mm) and focal length (40 mm). The low numerical aperture is suitable for three-dimensional imaging of cultured cells with single-cell resolution. Fig. 3(c) shows the z-axis profile of the OR-PAM image. The depth resolution of 47.30 ± 0.45 μm was determined as the full width at half maximum of the z-axis profile at 11 scan points. The B-scan rate of the image (4.87 Hz) was calculated as PRF/Nx/Nave, where PRF is the pulse repetition frequency, Nx is the number of sampling points along the x-axis, and Nave is the number of averagings.

4.3. Spectroscopic OR-PAM of a tube phantom

Fig. 4 shows the multispectral PAM images of tubes containing StellaFluor700 and IRDye800CW solutions. Fig. 4(a) and 4(b) show the maximum amplitude projection images of three-dimensional multispectral PAM images acquired using 50 nm bandwidth bandpass filters with central wavelengths of 700 nm and 800 nm, respectively. As shown in Fig. 4(c), StellaFluor700 and IRDye800CW exhibited absorption maxima at 706 nm and 796 nm, respectively. Therefore, the tube containing StellaFluor700 and IRDye800CW was imaged in Fig. 4(a) and (b), respectively. Fig. 4(d) shows the cross-sectional PA image acquired by the primary excitation light pulse of spectroscopic OR-PAM with 600–900 nm bandwidth excitation. The acoustic reflection is visible in the images due to the acoustic mismatching of the PTFE tube and water. The time was expressed on the vertical axis in Fig. 4(d) but can be converted to depth by multiplying sound speed and shifted to show the PA signal maximum at t = 0. Fig. 4(e) shows the cross-sectional PA image acquired by the secondary excitation light pulse. The time-axis of Fig. 4(e) was shifted 4.914 μs (time delay between the primary and secondary light pulses at 750 nm) from Fig. 4(d). Fig. 4(e) indicates that the time delay between the PA images produced by the primary and secondary light pulses was different for the different excitation wavelengths of the dyes. Fig. 4(f) shows the cross-correlation of the PA signals produced by the primary and secondary light pulses measured at the positions of the tubes containing StellaFluor700 and IRDye800CW

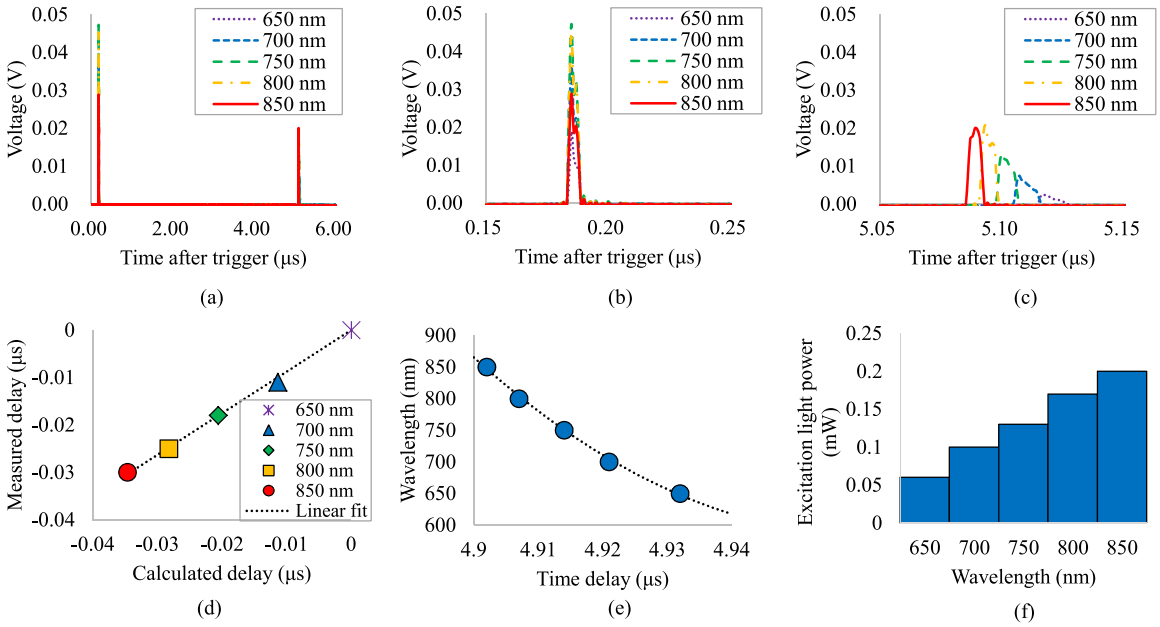

Fig. 2. The horizontal axes in (b) and (c) are in the same range ad were determined by the wavelength dependence of the time delay estimated from the chromatic aberration specification of the long SMF (approximately 0.15 ns/nm).
(a) Excitation light pulse emitted from the single-mode coupler triggered by a TTL synchronization output of the SC light source, (b) The magnified waveform of the primary light pulse, (c) The magnified waveform of the secondary light pulse, (d) Comparison of the calculated and measured time delays between the two pulses (plot, measurements, dotted line, linear fitting), (e) Wavelength dependence of the time delay between the first and second pulses (plot, measurements; dotted line, second-order poly-nominal fitting), and (f) Power of excitation light pulses at a repetition frequency of 100 kHz.

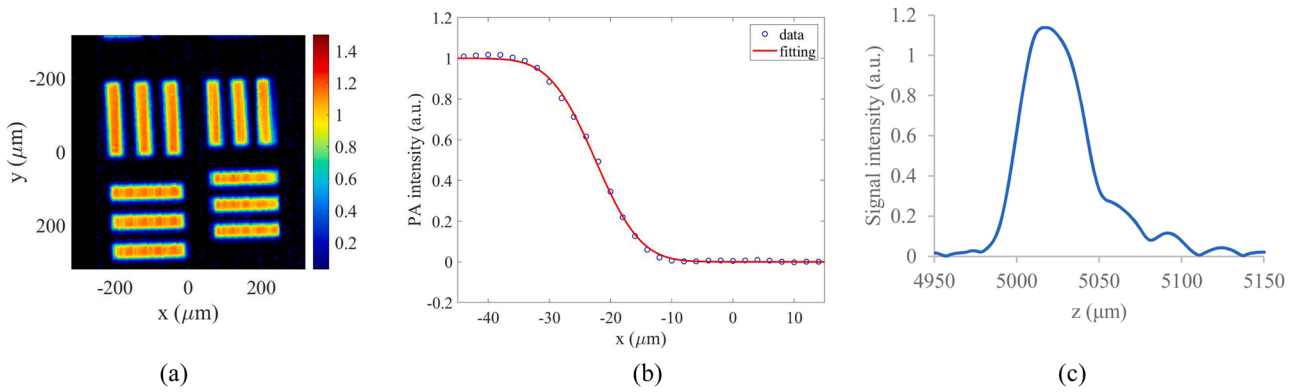

Fig. 3. (a) Maximum amplitude projection of the OR-PAM image of a chrome-coated test target. (b) Profile of the maximum amplitude projection of the OR-PAM image fitted to the edge-spread function (y = −80 μm). (c) Z-axis profile of the OR-PAM image (x = −40 μm, y = −80 μm).

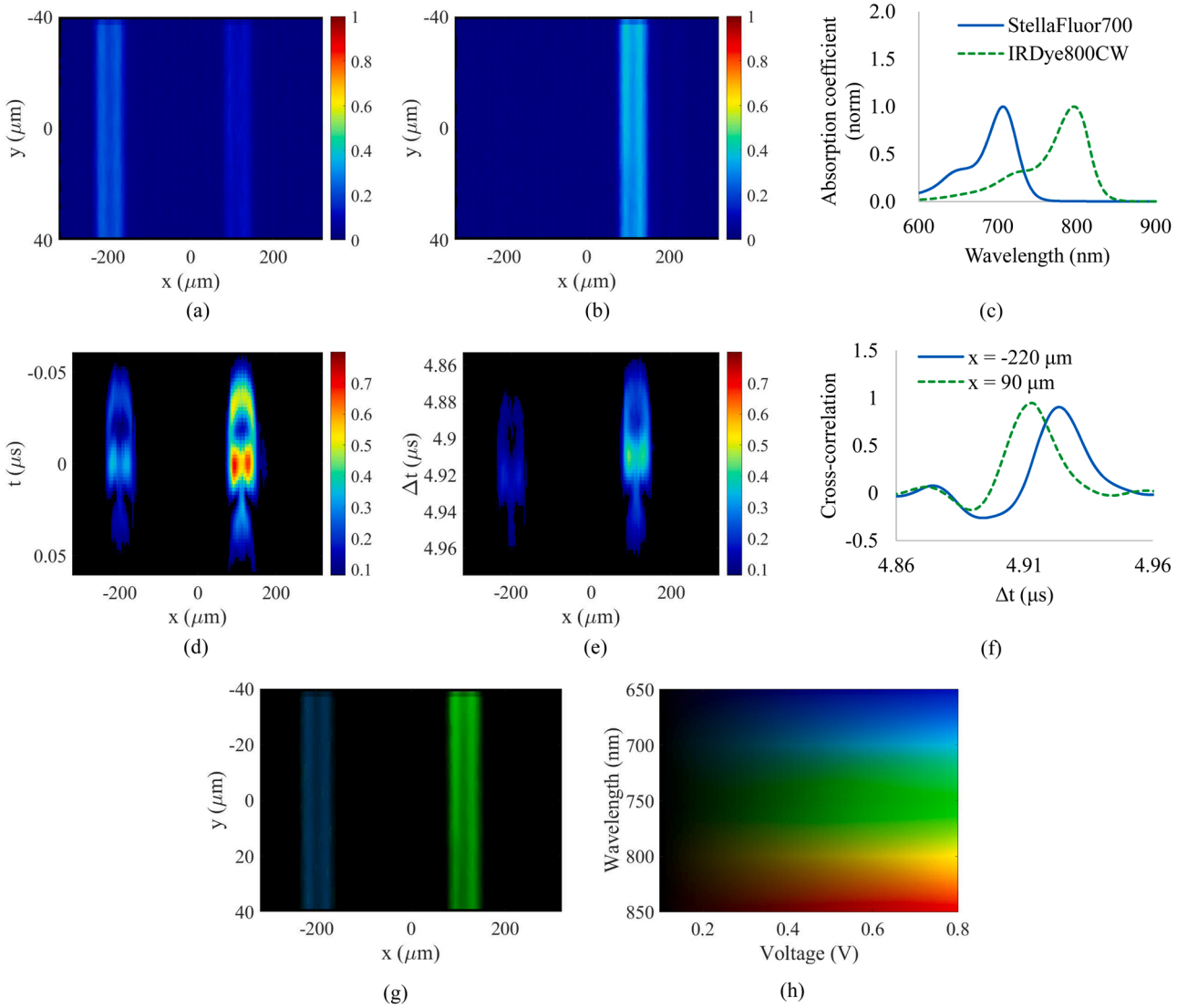

Fig. 4. (a) and (b) Maximum amplitude projection images of the three-dimensional multispectral PAM images of the two tubes containing Stellafluor700 (left tube) and IRDye800CW (right tube) solutions, acquired using bandpass filters with central wavelengths of (a) 700 nm and (b) 800 nm, respectively. (c) Absorption spectra of IRDye800CW and Stellafluor700 normalized by their absorption coefficients at their absorption peaks. Cross-sectional OR-PAM images were acquired without using a bandpass filter after the single-mode coupler produced by the (d) primary and (e) secondary light pulses. (f) Cross-correlation of the PA signals produced by the primary and secondary light pulses at x = −220 μm and 90 μm. (g) Spectroscopic OR-PAM image projected on the XY plane, and (h) colormap for the spectroscopic OR-PAM image expresses both excitation wavelength and PA signal intensity in a single image.

solutions. Considering the different excitation wavelengths of the dyes in each tube, the cross-correlations were maximized at different time delays. Fig. 4(g) shows the spectroscopic OR-PAM image indicating the PA signal intensity and excitation wavelengths using the colormap in Fig. 4(h). The figure shows that the proposed spectroscopic OR-PAM technique using wavelength-dependent time-delayed light pulses can differentiate between the two dyes inside the tubes. Fig. 4.

4.4. Spectroscopic OR-PAM of cultured cells

Fig. 5(a) and 5(b) show the cross-sectional OR-PAM images of the planar-cultured cell sample produced by the primary and secondary light pulses. As shown in Fig. 5(a), PA signals from the planar-cultured cells on the bottom of the dish were detected simultaneously from the primary light pulse irradiation. However, as shown in Fig. 5(b), PA signals from the planar-cultured cells on the bottom of the dish were detected at different time delays from the primary light pulse irradiation. The excitation wavelength was calculated by measuring the time delay of the PA signals produced from the primary and secondary light pulses. Fig. 5(c) shows the spectroscopic OR-PAM image that shows both the excitation wavelength and signal intensity. We used the four-color fluorescence microscopy image, as shown in Fig. 5(d), to compare the spectroscopic OR-PAM images and confirm the similarity between the spectroscopic OR-PAM and four-color fluorescence microscopy images, thus indicating that the proposed spectroscopic OR-PAM technique could differentiate the cell staining dyes based on the excitation wavelength. In spectroscopic OR-PAM, the numerical aperture of optical focusing should be lower than that of fluorescence microscopy to enable three-dimensional imaging with a considerable depth of field. Therefore, the spatial resolution of the spectroscopic OR-PAM image was lower than that of the fluorescence microscopy.

Fig. 6 shows the three-dimensional spectroscopic OR-PAM of Matrigel suspensions of the cells. In the z-stack spectroscopic OR-PAM image shown in Fig. 6(a), considering Matrigel-suspension-contained cells were stained using four different cell staining dyes, we detected cells with four different excitation wavelengths. Conversely, in the z-stack spectroscopic OR-PAM image of the Matrigel suspension containing cells stained using two cell staining dyes (Fig. 6(b) and(c)), we detected cells with two different excitation wavelengths. In the spectral dependence of the signal intensities shown in Fig. 6(d), the spectral peaks of each image correlated with the contents of the Matrigel suspension samples. Considering all samples exhibited a total cell concentration of 4×10^6 cells/mL, the concentration of the cells stained by each cell-staining dye were 1×10^6 cells/mL and 2×10^6 cells/mL in sample1, and sample2 and sample3, respectively. Therefore, the height of the spectral peaks was two times larger in sample2 and sample3, confirming that the proposed spectroscopic OR-PAM technique obtains data on the excitation wavelength for the samples even in three-dimensional imaging. Fig. 5.

5. Discussion

In this study, we proposed a new spectroscopic OR-PAM technique that uses the SC light source to acquire information on the excitation wavelength and PA signal intensity during single spatial scanning. First, we validated the optical system to produce two light pulses with and without wavelength-dependent time delays. Then, the technique was validated by imaging thin tubes containing dyes with different absorption spectra. Finally, three-dimensional spectroscopic OR-PAM of HeLa cells stained using cell-staining dyes were demonstrated. Fig. 6.

Fig. 4(g) shows that the proposed spectroscopic OR-PAM technique could differentiate between optical absorbers with different absorption

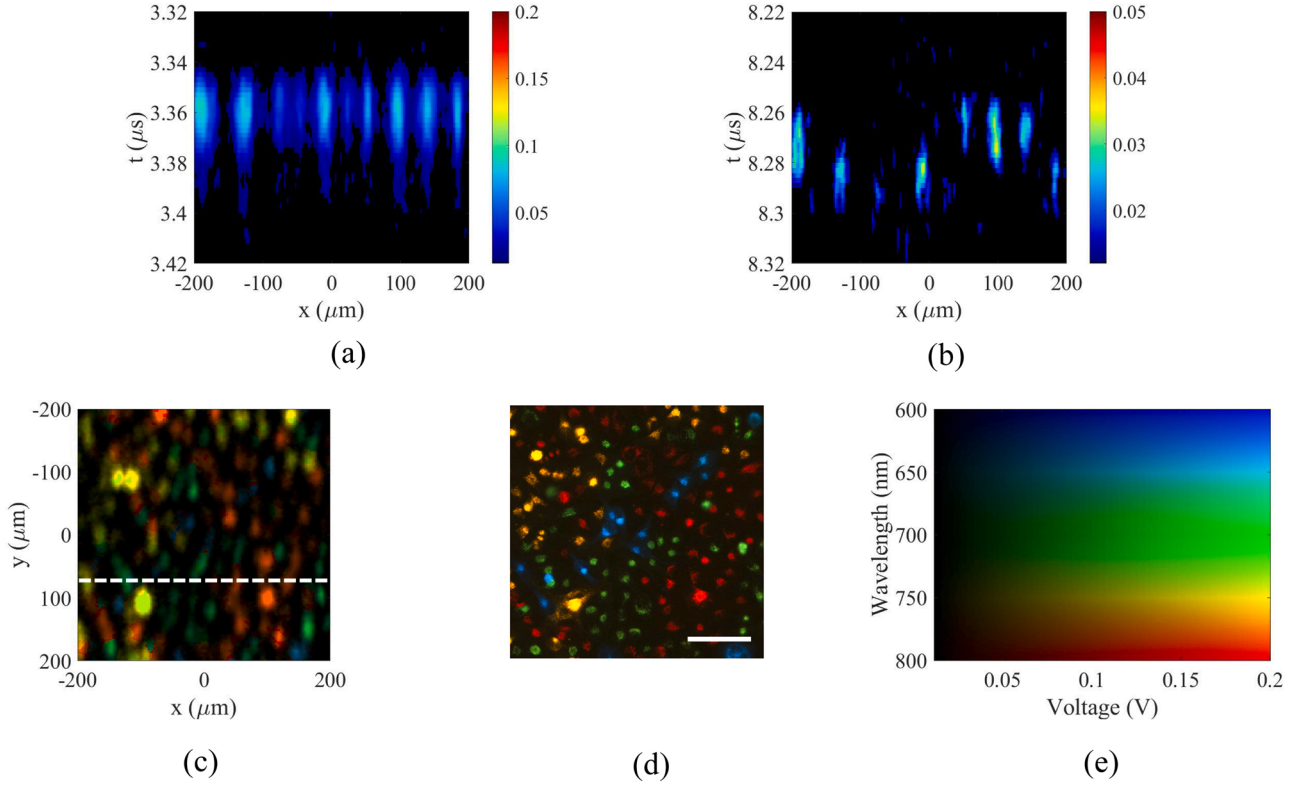

Fig. 5. Spectroscopic OR-PAM of the planar-cultured cells. (a) Cross-sectional OR-PAM image produced by the primary light pulses at slice y = −80 μm. (b) Cross-sectional OR-PAM image produced by the secondary light pulses at slice y = 80 μm. (c) Spectroscopic OR-PAM image of the cells. Dotted lines in the image indicate the lines corresponding to (a) and (b). (d) Four-color fluorescence microscope images of the cells stained by CellBrite Red (blue), CellBrite NIR680 (Green), CellBrite NIR750 (yellow), and CellBrite NIR790 (Red), and (e) colormap of the spectroscopic OR-PAM. Colorbar, 100 μm. (For interpretation of the references to colour in this figure legend, the reader is referred to the web version of this article.)

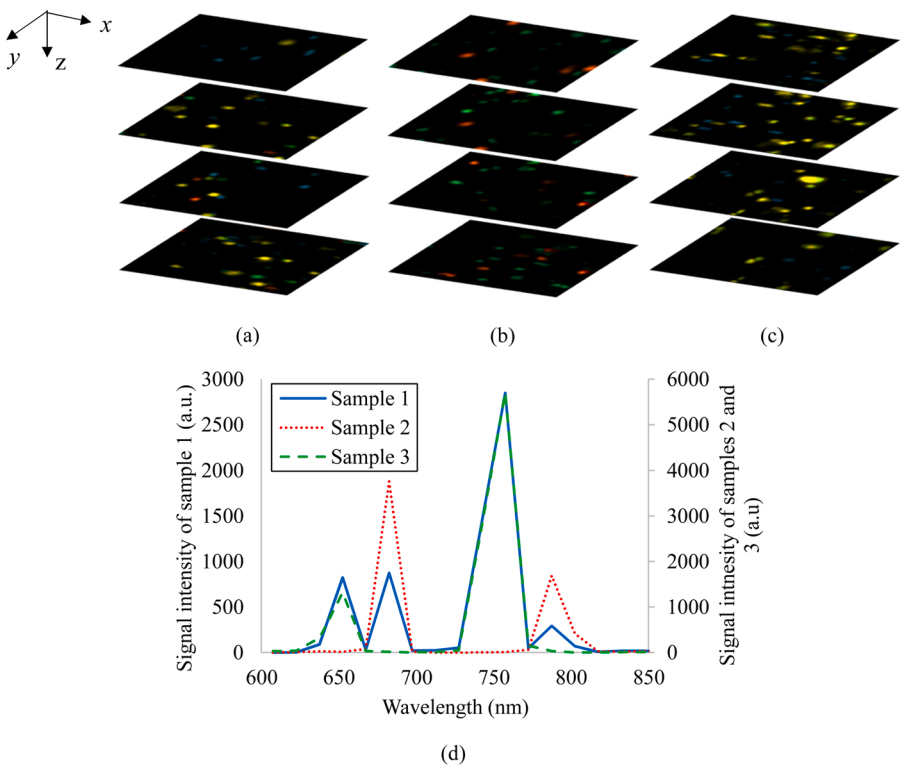

Fig. 6. Three-dimensional spectroscopic OR-PAM of cells dispersed in Matrigel. (a) z-stack image of sample 1 containing cells stained by CellBrite Red, CellBrite NIR680, CellBrite NIR750, and CellBrite NIR790; (b) z-stack image of sample 2 containing cells stained by CellBrite NIR680 and CellBrite NIR790; (c) z-stack image of sample 3 containing cells stained by CellBrite Red and CellBrite NIR750; (d) spectral dependence of the total signal intensities of the spectroscopic PAM images. The z-stack images were displayed with slice intervals of 120 μm and imaging areas of 280 × 280 μm each.

wavelengths during single spatial scanning. The excitation wavelengths of the tubes were calculated from the spectroscopic OR-PAM images shown in Fig. 4(g) as the average excitation wavelengths weighted by the signal intensities. The calculated excitation wavelengths were 689 nm and 763 nm, shorter than the absorption maxima of StellaFluor700 and IRDye800CW (706 nm and 796 nm), respectively. However, these values were close to the centroids of their absorption spectra (689 nm and 767 nm). Therefore, the excitation wavelengths determined by the spectroscopic OR-PAM technique reflected the centroids of the absorption spectra instead of the absorption maxima. The slight difference between the excitation wavelengths determined by the spectroscopic OR-PAM and centroids can be due to the excitation light spectrum, which originates from the output spectrum of the excitation light source and wavelength-dependent attenuation of the excitation light inside the long SMF. The optical attenuation inside the SMF was firmly wavelength-dependent due to the SMF core material's spectral characteristic and was relatively high at shorter wavelengths. The PA signal produced by the secondary light pulse was weighted by the spectrum of the secondary light pulse and resulted in errors in the excitation wavelength calculation. Although we have not compensated for the error, the spectroscopic OR-PAM successfully differentiated cells stained by various cell-staining dyes. However, compensation methods are needed to determine a more accurate excitation wavelength. One of the compensation methods is to use an optical filter to flatten the spectrum of the secondary light pulse. Alternatively, the error is corrected by calibrating the relationship between the excitation wavelength determined by spectroscopic OR-PAM and the actual excitation wavelength measured by standard methods. In another method, the wavelength dependence of the absorbed light energy b (λ) is calculated by performing the deconvolution process described in Eq. (7) and then divided by the spectrum of the secondary light pulse. Fig. 5(d) shows that the spectroscopic OR-PAM could differentiate between HeLa cells stained using four different cell-staining dyes. These results have been validated by comparing them with fluorescence microscope images. Since the differences in the excitation wavelengths of the four cell-staining dyes were at least 38 nm, we demonstrated that the spectroscopic OR-PAM had a spectral resolution of over 38 nm. The theoretical limit of the spectral resolution was determined from the sampling period of the oscilloscope and the dispersion characteristic of the SMF. As shown in Fig. 2(e), the time delay of the secondary pulse between 650 nm and 850 nm was 30 ns. Therefore, the averaged wavelength dispersion coefficient was 0.15 (ns/nm). The theoretical limit of the spectral resolution calculated by dividing the sampling rate of 2 ns by the averaged wavelength dispersion coefficient was 13.3 nm.

Three-dimensional spectroscopic OR-PAM is also demonstrated in Fig. 6(a)-(c). For three-dimensional imaging, the four cell-staining dyes were successfully differentiated. In the spectroscopic OR-PAM, the samples' depth position and spectral information were encoded in the time axis of the PA signal. However, due to this principle, the excitation wavelength could be misrecognized for high concentrations of optical absorbers. The excitation wavelength was calculated by evaluating the time delay that maximizes the cross-correlation of the PA signals produced from the primary and secondary pulses. The range of time delay search should be larger than the maximum wavelength dispersion of ± 22.5 ns, calculated as the product of the averaged wavelength dispersion coefficient and wavelength range (600–900 nm). If the optical absorbers are positioned farther than 67.5 μm (assuming that the speed of sound in water is 1500 m/s), the PA signals produced from the neighboring optical absorbers are not detected within the range of ± 22.5 ns, thus preventing misrecognition. This distance is the limiting factor of the axial resolution of the spectral processing to determine the excitation wavelength of the optical absorbers. The axial resolution of the spectral processing can be improved by limiting the excitation wavelength range or decreasing the wavelength dispersion coefficient. Since the spectral resolution can be improved as increasing the wavelength dispersion coefficient, the wavelength dispersion coefficient controls the trade-off between the axial resolution and the spectral resolution.

This study demonstrated that all-optical absorbers imaged by the spectroscopic OR-PAM had a single absorption band within the excitation wavelength range. However, optical absorbers with multiple absorption bands are not uncommon. In the case of an optical absorber

with multiple absorption bands within the excitation wavelength range, the cross-correlation function of the PA signals produced by the primary light pulse and the PA signals produced by the secondary light pulse has multiple peaks due to the numerous absorption bands. In the proposed method, the wavelength corresponding to the highest peak of the cross-correlation function is determined as the excitation wavelength for the maximum cross-correlation function. This can result in a loss of information about the optical absorber. By detecting multiple peaks in the cross-correlation function, the excitation wavelengths for each absorption band become apparent when they are well spaced in the spectrum. The proposed spectroscopic OR-PAM technique is advantageous concerning wavelength tunability compared with existing multispectral OR-PAM. While the excitation light is limited to laser wavelengths in existing multispectral OR-PAM, the excitation wavelength range can be adjusted in the spectroscopic OR-PAM with SC light sources using BPFs. To our best knowledge, a near-infrared wavelength-tunable nanosecond pulsed laser with hundreds of kHz repetition frequency is not commercially available. Therefore, multispectral OR-PAM systems can image contrast agents with near-infrared excitation wavelengths are extremely limited. Therefore, the proposed spectroscopic OR-PAM using SC light source enables the application of OR-PAM in the near-infrared wavelength range due to low intrinsic signal intensity and relatively low optical scattering. Additionally, it provides continuous wavelength measurement. The OR-PAM images must be corrected at multiple excitation wavelengths to differentiate multiple optical absorbers in existing multispectral OR-PAM. However, lasers are needed for each excitation wavelength, and spatial scanning should be repeated in this case. Conversely, in the spectroscopic OR-PAM, continuous spectral information, e.g., hyper-spectral imaging, is acquired during single spatial scanning and helps in four-color OR-PAM imaging in the 600–850 nm (Figs. 5 and 6). The near-infrared wavelengths are advantageous for contrast agent imaging because of their low optical attenuation and low intrinsic signal intensity mainly caused by hemoglobin. Thus, the four-color volumetric OR-PAM may be useful for in vivo tracking of four different cells to analyze intercellular interactions in tissues. Furthermore, the potentially high throughput is the spectroscopic OR-PAM technique that can offer spectroscopic information during single spatial scanning. In transmission-mode OR-PAM with motorized stage scan, the imaging speed is limited by the slow scan speed of the motorized stage. However, this technique can be combined with the reflection-mode PAM with fast scanning techniques that use MEMS mirrors [13] or polygonal mirrors [15]. As a result, the spectroscopic OR-PAM improves the throughput of multispectral PAM by rejecting the repetition of spatial scanning to correct the spectral information. In addition, the spectroscopic OR-PAM is theoretically robust against motion artifacts. In conventional multispectral OR-PAM with multiple spatial scanning, displacements of the optical absorbers during multiple spatial scanning cause motion artifacts and result in inaccurate spectral processing. These benefits are useful for applications that collect dynamic information from biological tissues, such as multicolor tracking of cells circulating in the blood vessels.

One of the main limitations of this technique is the attenuation of excitation light. In the single-mode coupler used to separate the primary and secondary light pulses, the light emitted to one of two optical outputs was dumped, causing a 50% loss of light energy. Additionally, due to silica's relatively high attenuation coefficient at a wavelength of 650 nm, the excitation light was attenuated by 10 dB in the long SMF. Therefore, the excitation light emitted from the SMF was attenuated by approximately 5% of the input at the output of the single-mode coupler at 650 nm. This low transmission efficiency limited the excitation light pulse energy and consequently limited the signal-to-noise ratio. Upon improving the transmission efficiency, the throughput of the spectroscopic OR-PAM can be improved by reducing the signal averaging. Another limitation of this technique is the excitation efficiency, i.e., PA signal intensity per light pulse energy. The excitation efficiency of broadband light pulses is lower than that of narrowband light pulses. The broadband excitation light pulse contains wavelength content that is not absorbed by the optical absorbers and consequently does not contribute to PA signal generation because the absorption spectra of the optical absorbers are generally narrower than the bandwidth of the excitation light pulse. Thus, as the bandwidth of the excitation light pulse increases, the excitation efficiency decreases. The pulse energy per irradiation area regulates the safety limit. Therefore, the decrease in excitation efficiency reduces the PA signal intensity produced by the excitation light pulses with the safety limit energy. This problem limits the signal-to-noise ratio of the proposed spectroscopic OR-PAM. A bandpass filter can easily adjust the excitation bandwidth of the spectroscopic OR-PAM. Thus, it is essential to select an optimum balance for the trade-off between the excitation efficiency and bandwidth depending on the application.

6. Conclusion

In this study, we proposed a novel spectroscopic OR-PAM technique for obtaining dual information of excitation wavelength and PA signal intensity during single spatial scanning. In the proposed spectroscopic OR-PAM, excitation light pulses produced from SC light source were split into broadband excitation light pulses with and without wavelength-dependent time delays and irradiated on samples. The excitation wavelengths of the samples were determined by measuring the time delay between the PA signals produced between the two light pulses. The excitation light pulses were successfully produced using single-mode couplers and a long SMF. Furthermore, the theory of spectroscopic measurement was validated by measuring dye solutions. Lastly, we successfully demonstrated the three-dimensional spectroscopic OR-PAM imaging of cells stained using different cell-staining dyes. Although there is a limitation about the trade-off between excitation efficiency and excitation bandwidth, optimizing the excitation bandwidth depending on the application is possible. The proposed spectroscopic OR-PAM improves the throughput of spectroscopic signal acquisition by removing the wavelength scan performed in most existing multispectral OR-PAM techniques. Therefore, combining the proposed technique with fast spatial scanning techniques can significantly contribute to recent OR-PAM applications, such as monitoring quick biological events and microscale tracking of moving materials.

Funding

This work was supported by a Grant-in-Aid for Scientific Research on Innovative Areas "Singularity Biology (No. 8007)" (21H00445 to MI, 19H05436 to MI) of MEXT, a JSPS KAKENHI Grant Number 19K12856 to TH, SO, and MI, Defense Medicine Basic Research Program (A) to MI, SO, and TH, Defense Medicine Basic Research Program (C) to TH, Nippon Sheet Glass Foundation of Materials Science and Engineering to MI.

Declaration of Competing Interest

The authors declare that they have no known competing financial interests or personal relationships that could have appeared to influence the work reported in this paper.

Acknowledgments

The authors thank H. Sanguu (Yokogawa Electric Corporation) for his essential advice regarding this research and A. Shito, Y. Inoue, and Y. Tabata (SigmaKoki Co., LTD) for their assistance with the optical design. The authors would also like to thank K. Tsujita for his essential contributions to this work.

References

[1] S. Hu, K. Maslov, L.V. Wang, Second-generation optical-resolution photoacoustic microscopy with improved sensitivity and speed, Opt. Lett. 36 (7) (2011) 1134–1136.
[2] J. Yao, L.V. Wang, Photoacoustic microscopy, Laser Photonics Rev. 7 (5) (2013) 758–778.
[3] K. Maslov, H.F. Zhang, S. Hu, L.V. Wang, Optical-resolution photoacoustic microscopy for in vivo imaging of single capillaries, Opt. Lett. 33 (9) (2008) 929–931.
[4] J. Yao, K.I. Maslov, Y. Zhang, Y. Xia, L.V. Wang, Label-free oxygen-metabolic photoacoustic microscopy in vivo, J. Biomed. Opt. 16 (7) (2011) 076003–076003-11.
[5] L. Wang, K. Maslov, L.V. Wang, Single-cell label-free photoacoustic flowoxigraphy in vivo, Proc. Natl. Acad. Sci. 110 (15) (2013) 5759–5764.
[6] T. Liu, Q. Wei, J. Wang, S. Jiao, H.F. Zhang, Combined photoacoustic microscopy and optical coherence tomography can measure metabolic rate of oxygen, Biomed. Opt. Express 2 (5) (2011) 1359–1365.
[7] W. Song, Q. Wei, W. Liu, T. Liu, J. Yi, N. Sheibani, A.A. Fawzi, R.A. Linsenmeier, S. Jiao, H.F. Zhang, A combined method to quantify the retinal metabolic rate of oxygen using photoacoustic ophthalmoscopy and optical coherence tomography, Sci. Rep. 4 (2014) 6525.
[8] Y. Wang, K. Maslov, Y. Zhang, S. Hu, L. Yang, Y. Xia, J. Liu, L.V. Wang, Fiber-laser-based photoacoustic microscopy and melanoma cell detection, J. Biomed. Opt. 16 (1) (2011) 011014–011014-4.
[9] Y. He, L. Wang, J. Shi, J. Yao, L. Li, R. Zhang, C.-H. Huang, J. Zou, L.V. Wang, In vivo label-free photoacoustic flow cytography and on-the-spot laser killing of single circulating melanoma cells, Sci. Rep. 6 (2016) 39616.
[10] J. Chen, Y. Zhang, X. Li, J. Zhu, D. Li, S. Li, C.-S. Lee, L. Wang, Confocal visible/NIR photoacoustic microscopy of tumors with structural, functional, and nanoprobe contrasts, Photonics, Research 8 (12) (2020) 1875–1880.
[11] J. Chen, Y. Zhang, L. He, Y. Liang, L. Wang, Wide-field polygon-scanning photoacoustic microscopy of oxygen saturation at 1-MHz A-line rate, Photoacoustics 20 (2020), 100195.
[12] Y. He, J. Shi, K.I. Maslov, R. Cao, L.V. Wang, Wave of single-impulse-stimulated fast initial dip in single vessels of mouse brains imaged by high-speed functional photoacoustic microscopy, J. Biomed. Opt. 25 (6) (2020), 066501.
[13] J.Y. Kim, C. Lee, K. Park, G. Lim, C. Kim, Fast optical-resolution photoacoustic microscopy using a 2-axis water-proofing MEMS scanner, Sci. Rep. 5 (2015) 7932.
[14] K. Park, J.Y. Kim, C. Lee, S. Jeon, G. Lim, C. Kim, Handheld photoacoustic microscopy probe, Sci. Rep. 7 (1) (2017) 1–15.
[15] B. Lan, W. Liu, Y.-c Wang, J. Shi, Y. Li, S. Xu, H. Sheng, Q. Zhou, J. Zou, U. Hoffmann, High-speed widefield photoacoustic microscopy of small-animal hemodynamics, Biomed. Opt. Express 9 (10) (2018) 4689–4701.
[16] S.M. Park, S.-W. Cho, B.-M. Kim, T.G. Lee, C.-S. Kim, S.-W. Lee, Quickly alternating green and red laser source for real-time multispectral photoacoustic microscopy, Photoacoustics 20 (2020), 100204.
[17] T. Wang, N. Sun, R. Cao, B. Ning, R. Chen, Q. Zhou, S. Hu, Multiparametric photoacoustic microscopy of the mouse brain with 300-kHz A-line rate, Neurophotonics 3 (4) (2016), 045006.
[18] H. Kang, S.W. Lee, S.M. Park, S.W. Cho, J.Y. Lee, C.S. Kim, T.G. Lee, Real-time functional optical-resolution photoacoustic microscopy using high-speed alternating illumination at 532 and 1064 nm, J. biophotonics 11 (3) (2018), e201700210.
[19] C. Liu, J. Chen, Y. Zhang, J. Zhu, L. Wang, Five-wavelength optical-resolution photoacoustic microscopy of blood and lymphatic vessels, Adv. Photonics 3 (1) (2021), 016002.
[20] Y. Zhou, S. Liang, M. Li, C. Liu, P. Lai, L. Wang, Optical-resolution photoacoustic microscopy with ultrafast dual-wavelength excitation, J. biophotonics 13 (6) (2020), e201960229.
[21] S.-W. Cho, S.M. Park, B. Park, T.G. Lee, B.-M. Kim, C. Kim, J. Kim, S.-W. Lee, C.-S. Kim, High-speed photoacoustic microscopy: a review dedicated on light sources, Photoacoustics 24 (2021), 100291.
[22] M. Bondu, C. Brooks, C. Jakobsen, K. Oakes, P.M. Moselund, L. Leick, O. Bang, A. Podoleanu, High energy supercontinuum sources using tapered photonic crystal fibers for multispectral photoacoustic microscopy, J. Biomed. Opt. 21 (6) (2016), 061005-061005.
[23] M. Bondu, M. Marques, P.M. Moselund, G. Lall, A. Bradu, A. Podoleanu, Multispectral photoacoustic microscopy and optical coherence tomography using a single supercontinuum source, Photoacoustics 9 (2018) 21–30.
[24] X. Shu, M. Bondu, B. Dong, A. Podoleanu, L. Leick, H.F. Zhang, Single all-fiber-based nanosecond-pulsed supercontinuum source for multispectral photoacoustic microscopy and optical coherence tomography, Opt. Lett. 41 (12) (2016) 2743–2746.
[25] M. Bondu, M. Denninger, P.M. Moselund, A. Podoleanu, Using a single supercontinuum source for visible multispectral photoacoustic microscopy and 1300 nm optical coherence tomography, European Conference on Biomedical Optics, Optical Society of America, 2017, p. 1041507.
[26] M.K. Dasa, G. Nteroli, P. Bowen, G. Messa, Y. Feng, C.R. Petersen, S. Koutsikou, M. Bondu, P.M. Moselund, A. Podoleanu, All-fibre supercontinuum laser for in vivo multispectral photoacoustic microscopy of lipids in the extended near-infrared region, Photoacoustics 18 (2020), 100163.
[27] C. Lee, S. Han, S. Kim, M. Jeon, M.Y. Jeon, C. Kim, J. Kim, Combined photoacoustic and optical coherence tomography using a single near-infrared supercontinuum laser source, Appl. Opt. 52 (9) (2013) 1824–1828.
[28] T. Buma, N.C. Conley, S.W. Choi, Multispectral photoacoustic microscopy of lipids using a pulsed supercontinuum laser, Biomed. Opt. Express 9 (1) (2018) 276–288.
[29] Y. Chang, Y. Hu, Z. Chen, D. Xing, Co-impulse multispectral photoacoustic microscopy and optical coherence tomography system using a single supercontinuum laser, Opt. Lett. 44 (18) (2019) 4459–4462.
[30] K. Tachi, T. Hirasawa, S. Okawa, A. Horiguchi, K. Ito, M. Ishihara, Chromatic-aberration-free multispectral optical-resolution photoacoustic microscopy using reflective optics and a supercontinuum light source, Appl. Opt. 60 (31) (2021) 9651–9658.
[31] J. Yao, L.V. Wang, Sensitivity of photoacoustic microscopy, Photoacoustics 2 (2) (2014) 87–101.
[32] C. Li, L.V. Wang, Photoacoustic tomography and sensing in biomedicine, Phys. Med. Biol. 54 (19) (2009) R59.
[33] T. Hirasawa, M. Fujita, S. Okawa, T. Kushibiki, M. Ishihara, Quantification of effective attenuation coefficients using continuous wavelet transform of photoacoustic signals, Appl. Opt. 52 (35) (2013) 8562–8571.
[34] Y. Wang, D. Xing, Y. Zeng, Q. Chen, Photoacoustic imaging with deconvolution algorithm, Phys. Med. Biol. 49 (14) (2004) 3117.
[35] Y. Wang, R. Wang, Photoacoustic recovery of an absolute optical absorption coefficient with an exact solution of a wave equation, Phys. Med. Biol. 53 (21) (2008) 6167.
[36] Z. Guo, S. Hu, L.V. Wang, Calibration-free absolute quantification of optical absorption coefficients using acoustic spectra in 3D photoacoustic microscopy of biological tissue, Opt. Lett. 35 (12) (2010) 2067–2069.
[37] Z. Guo, C. Favazza, A. Garcia-Uribe, L.V. Wang, Quantitative photoacoustic microscopy of optical absorption coefficients from acoustic spectra in the optical diffusive regime, J. Biomed. Opt. 17 (6) (2012) 0660111–0660116.
[38] T.S. Sazzad, S. Islam, Use of gamma encoder on HSL color model improves human visualization in the field of image processing, Int. J. Comput. Sci. Eng. 2 (5) (2013) 177–182.
[39] T. Hirasawa, R.J. Iwatate, M. Kamiya, S. Okawa, Y. Urano, M. Ishihara, Multispectral photoacoustic imaging of tumours in mice injected with an enzyme-activatable photoacoustic probe, J. Opt. 19 (1) (2017), 014002.
[40] S. Jeon, J. Kim, D. Lee, B.J. Woo, C. Kim, Review on practical photoacoustic microscopy, Photoacoustics (2019), 100141.

Takeshi Hirasawa received B.S. and M.S. degrees from Nagaoka University of Technology in 2008 and 2010, and a Ph. D. degree from Meiji University in 2019, respectively. He is currently an assistant professor at Department of Medical Engineering, National Defense Medical College. His research interest includes photoacoustic imaging and photoacoustic microscopy.

Kazuyoshi Tachi graduated from National Defense Medical College, received M.D. degree and qualified as a medical doctor in 2009. Then he started serving as a medical officer of the Maritime Self-Defense Force. In 2018, he enrolled in a doctoral course of National Defense Medical College.

Shinpei Okawa received a Ph.D. degree in Applied Physics from Keio University in 2006. In 2006, he joined Department of Mechanical Engineering and Intelligent Systems at the University of Electro-Communications as an Assistant professor. From 2012–2021, he worked at Department of Medical Engineering, National Defense Medical College as an Assistant professor. He is currently a professor at Preeminent Medical Photonics Education and Research Center, Hamamatsu University School of Medicine. His research interests include image reconstruction and signal processing in biomedical optics.

Toshihiro Kushibiki , Ph.D. Associate Professor, Department of Medical Engineering, National Defense Medical College, Japan.Toshihiro Kushibiki (TK) has consistently progressed research in the interdisciplinary fields of materials engineering and medical applications of photochemistry and photobiology. TK has received various awards in recognition of their research results and achievements. TK is also working to integrate and develop research results and to create and pioneer new research fields that incorporate new concepts and methods.

Miya Ishihara received the M.S. degrees from Keio University, Japan in 1994, and received the Ph.D. degree from Kitasato University, Japan in 2002. In 1996, she accepted a post at Department of Medical Engineering, National Defense Medical College, where she served as an Associate Professor since 2006 and a Professor since 2011. Dr. Ishihara received the Best oral presentation Award of the 5th Meeting of the Tissue Engineering Society International (2002), the Young investigator's Award (2003) and the Best research award (2006) of Japan Society of Medical and Biological Engineering, and the Best presentation of the 79th Japanese society of medical instrumentation (2004).